Clim. Past Discuss., 9, 329–350, 2013
www.clim-past-discuss.net/9/329/2013/
doi:10.5194/cpd-9-329-2013

Climate of the Past Discussions

A Last Glacial Maximum World-Ocean simulation at eddy-permitting resolution – Part 2: Confronting the paleo-proxy data

M. Ballarotta[1], **K. Döös**[1], **P. Lundberg**[1], **L. Brodeau**[1], **and J. Brandefelt**[2]

[1]Department of Meteorology/Oceanography, Stockholm University, 106 91 Stockholm, Sweden
[2]Department of Mechanics, KTH (Royal Institute of Technology), 106 91 Stockholm, Sweden

Received: 21 December 2012 – Accepted: 4 January 2013 – Published: 18 January 2013

Correspondence to: M. Ballarotta (maxime@misu.su.se)

Published by Copernicus Publications on behalf of the European Geosciences Union.

Abstract

Previous investigations concerning the design of an eddy-permitting LGM oceanic simulation are here extended with focus on whether this type of simulation is capable of improving the numerical results with regard to the available paleo-proxy reconstructions. Consequently, an eddy-permitting and two coarse-grid simulations of the same LGM period are confronted with a dataset from the Multiproxy Approach for the Reconstruction of the Glacial Ocean Sea Surface Temperatures (MARGO SSTs) and a number of sea-ice reconstructions. From a statistical analysis it was found that the eddy-permitting simulation does not significantly improve the SST representation with regard to the paleo-reconstructions. The western boundary currents are better resolved in the high-resolution experiment than in the coarse simulations, but, although these more detailed SST structures yield a locally improved consistency between modelled predictions and proxies, they do not contribute significantly to the global statistical score. As in the majority of the PMIP2 simulations, the modelled sea-ice conditions are still inconsistent with the paleo-reconstructions, probably due to the choice of the model equilibrium.

1 Introduction and motivation

Because of its proximity to the present day, the Last Glacial Maximum is a particularly useful time-slice of the earth's climate history for testing numerical models under glacial boundary conditions. Additionally, the availability of reconstructed surface temperatures and sea-ice extent from paleo-archives offer the possibility of evaluating these models. However, these proxy-data pertain to discrete source points and are thus only valid over a specific spatial scale, which usually is smaller than the resolution of the climate-model grids (Hargreaves et al., 2011). A comparison between the coarse-resolution climate simulation and the reconstructed sea-surface state indicated that the ensemble of PMIP models designed under the Paleoclimate Modelling Intercomparison

CPD
9, 329–350, 2013

Projects can be regarded as globally reliable with respect to the Multiproxy Approach for the Reconstruction of the Glacial Ocean surface (MARGO) Sea Surface Temperature (SST) data synthesis (Waelbroeck et al., 2009) for the Last Glacial Maximum (LGM) (Hargreaves et al., 2011, 2012). On the other hand, it has been noted that although these models reproduce the strong SST meridional gradients and the cooling in the North Atlantic, they sometimes do not place the gradients at the right location or fail in estimating the magnitude of the regional cooling (Kageyama et al., 2006; Otto-Bliesner et al., 2009; Braconnot et al., 2012).

The realism of the results from model simulations of the Last Glacial Maximum conducted during the PMIP2 project has also been discussed in the IPCC Fourth Assessment Report (IPCC AR4 – FAQ6.1: how Realistic Are Results from Climate Model Simulations of the Last Glacial Maximum?). Here it is mentioned that even if "the PMIP-2 LGM simulations confirm that current AOGCMs are able to simulate the broad-scale spatial patterns of regional climate change recorded by palaeo data in response to the radiative forcing and continental ice sheets of the LGM", still, "Regional variations in simulated tropical cooling are much smaller than indicated by MARGO data, partly related to models at current resolutions being unable to simulate the intensity of coastal upwelling and eastern boundary currents."

It will hence be useful to evaluate whether high-resolution modelling, e.g. eddy-permitting oceanic simulations, improve the representation of the surface state compared to coarse-resolution models and the paleo-proxy reconstructions. In this study, we confront three model experiments (one coarse-resolution forced ocean simulation, one coarse-resolution climate simulation, and one eddy-permitting simulation) with the available recent reconstructions of the surface state of the glacial ocean. By applying statistical analysis to the datasets, we estimate the accuracy of each type of simulation in representing the reconstructed surface state.

CPD
9, 329–350, 2013

2 Methods

The accompanying Part 1 of the present study (Ballarotta et al., 2013) described the behaviour of a NEMO-based (Madec, 2008) eddy-permitting simulation forced by a prescribed LGM atmospheric state constructed from a quasi-equilibrated CCSM3 climate simulation (Brandefelt and Otto-Bliesner, 2009). It was concluded that this eddy-permitting simulation more-or-less closely represented the LGM state simulated with the CCSM3 climate model by Brandefelt and Otto-Bliesner (2009), but showed discrepancies as regards the sea-ice area, the North Atlantic surface temperatures, the site of deep-water formation, and the global salinity simulated by the PMIP models. The simulated ocean-surface state from the eddy-permitting experiment is in the present study compared with the MARGO dataset (Waelbroeck et al., 2009). This a compilation of almost 700 samples located especially in the North Atlantic, the Southern Ocean and the Tropical region. These data are reconstructions of the annual mean (hereafter ANN), the boreal winter (January-February-March, JFM) and the boreal summer (July-August-September, JAS).

To evaluate the effects of the model-grid resolution, two coarsely resolved simulations are added to the comparison with the proxy-data: the model outputs from the source CCSM3 simulation and a NEMO-based coarse-resolution simulation implementing the same boundary conditions as in its NEMO eddy-permitting counterpart. Consequently, the three models (hereafter, eddy-permitting NEMO-ORCA025, coarse-resolution NEMO-ORCA1 and CCSM3) represent the same simulated period with the same atmospheric forcing. A summary of the three experiments is given in Table 1.

The annual-mean, the boreal-winter and -summer SSTs are examined for each source point from the MARGO dataset. The comparison is made by taking the results at the model grid-box coordinates closest to the location of the proxy data-point. The performance of the models can then be evaluated by their skill and illustrated using the Taylor-diagram representation (Taylor, 2001), which diagnoses the correlation between model and data, the RMS difference and field standard deviation. The former quantity

CPD
9, 329–350, 2013

is a statistical measure of the accuracy of the model in representing the surface state, which is assumed to be perfect. A formal definition is given by Taylor (2001):

$$S = \frac{4(1+R)}{(\hat{\sigma}_f + 1/\hat{\sigma}_f)^2(1+R_0)}, \quad (1)$$

where R is the correlation coefficient, $\hat{\sigma}_f$ the ratio between the model variance and the MARGO dataset variance, and R_0 the maximum correlation attainable. In our cases, the reference fields are the MARGO annual-mean, boreal-winter (JFM) and boreal-summer (JAS) SSTs, while the "test" fields are the model outputs. The skill scores are defined with R_0 set equal to 1, i.e. when the model results exactly fit the reconstruction. A skill score of 1 means that the model performs well while 0 is a bad score. Finally, the Taylor diagrams are evaluated over four latitudinal bands (50–25° S, 25° S–25° N, 25–50° N and 50–90° N) to isolate the regional changes due to the introduction of the permitted eddies.

3 Effect of the model resolution

3.1 On the surface temperature

Between 50 and 90° N (Fig. 1), the three model outputs are uncorrelated with the MARGO reconstruction. The correlation coefficients are smaller than 0.25 for all of the ANN, JFM and JAS data. Moreover, the standard deviations of the simulated SSTs are close to zero, suggesting that the simulated SSTs in this region are relatively homogenous (viz. a small variability of the SSTs). As a result, the zonal SST gradients in the North Atlantic (Waelbroeck et al., 2009) from the MARGO reconstruction are not resolved by the models. The reason for this mismatch between the model results and the proxy data can be explained by the presence of large sea-ice covers in each of the simulations, which is a characteristic of the model-equilibrated period (Brandefelt and Otto-Bliesner, 2009). Consequently, the RMSE is between 3.0 and

CPD
9, 329–350, 2013

4.5 °C and the skill scores are close to zero (Table 2), i.e. the three models fail to represent the SSTs in this region.

Between 25 and 50° N (Fig. 2), the three models show similar behaviour. They capture the variability of the SSTs, but the correlation coefficients are between 0.7 and 0.8 for the annual-mean and summer reconstructions and between 0.8 and 0.9 for the winter reconstruction. Note that the coarse-resolution simulations (ORCA1 and CCSM3) have the best correlation and RMSE with the annual-mean and winter reconstructions, whereas ORCA025 is slightly better than CCSM3 for the boreal-summer months. The skill scores of the models are between 0.83 and 0.95.

Between 25° S and 25° N (Fig. 3), the models underestimate the variability of the MARGO SSTs. Again, they show similar behaviour, which, in view of the available proxy-data, is not in favour of the high-resolution simulation. For each reconstruction, the correlation coefficient is near 0.6, the RMSE slightly above 3 °C and the skill scores above 0.5.

Between 25 and 50° S (Fig. 4), the correlation is extremely good with regards to the paleo-reconstruction. The correlation coefficients are between 0.95 and 0.99. However, the RMSE is around 2 °C. In this region, the three models have the same skill scores: 0.97 for the annual mean reconstruction, 0.98 for JFM and 0.97 for JAS.

The present analysis shows that for each latitudinal band the coarse-resolution and eddy-permitting simulations have similar skills. For a closer look at the local impact of high resolution, the boreal-summer SST maps in the Agulhas, North-Atlantic and Kuroshio regions are shown in Figs. 5, 6 and 7, respectively. The JAS SST values and locations of the MARGO data are superimposed. The conclusions are drawn for the summer months, but are also valid for the annual mean and the boreal-winter months (and hence the analogous annual-mean and boreal-winter maps are not shown). These maps show that the structure of the simulated SSTs may differ locally between the coarse and the eddy-permitting simulation, which can increase or decrease the correlation with the MARGO dataset. In the Agulhas region, the width of the Agulhas current along the coast of Mozambique and South Africa is narrower in the eddy-permitting

CPD
9, 329–350, 2013

simulation. Moreover, the meandering of the Antarctic Circumpolar Current (ACC) is more distinct when eddies are permitted. As a consequence, the meridional SST gradients in these regions are better captured by the ORCA025 experiment. In the Gulf Stream region, the ORCA1 experiment appears to be in better agreement with the available proxy-data, whereas in the Kuroshio region, the ORCA025 simulation is slightly closer to the reconstruction.

3.2 On the sea-ice extent

In addition to the SST reconstruction, sea-ice reconstructions are available for the LGM period (Pflaumann et al., 2003; De Vernal et al., 2006; Nørgaard-Pedersen et al., 2003; Gersonde et al., 2005). For the boreal-winter months (Fig. 8), the models simulate sea-ice cover in the northwestern North Atlantic and in the Labrador as well as Nordic Seas. However, this North Atlantic sea-ice extent reaches almost 40° N, whereas the margin is located between 50 and 60° N in the reconstructions (Pflaumann et al., 2003; De Vernal et al., 2006). The ice-free conditions in the Irminger current up to Iceland are also less pronounced in our simulation. In the Southern Ocean, the models simulate a larger sea-ice extent than in the proxy reconstructions (Gersonde et al., 2005). The sea-ice edge is located near 50° S between 60° W and 120° E and near 55° S in the rest of the circumpolar region. For the boreal summer (Fig. 9), the LGM sea-ice fractions are reduced in the Labrador Sea, the Central North Atlantic and the Norwegian Sea, suggesting possibly ice-free conditions during the glacial period (cf. the animation available as supplemental material). The central Arctic basin and western Fram Strait have perennial sea-ice, in accordance with Nørgaard-Pedersen et al. (2003). In the Southern Ocean, the modelled maximal sea-ice area is around 39×10^6 km^2 (not shown), which is similar to the reconstruction (Gersonde et al., 2005) with sea-ice extending to around 45° S in the Atlantic and Indian Oceans and 55° S in the Pacific. Finally, it is important to note that a large Southern-Ocean seasonality is observed for the region fully covered by sea-ice but not for the sea-ice margin (in the Supplement, the 100 %

CPD
9, 329–350, 2013

isoline reaches as far as 52° S during the austral winter and 60 to 65° S during the austral summer).

4 Conclusions

A companion study by Ballarotta et al. (2013) described the motivation for designing an eddy-permitting ocean experiment and reported a basic evaluation of the model response. Using an atmospheric state from a quasi-equilibrated climate simulation, it was shown that the high-resolution forced ocean simulation was capable of reproducing the glacial state from the source simulation. The present study deals with the prospects of the eddy-permitting simulation to be in better agreement with the paleo-proxy data, which was investigated on the basis of a comparison with two coarse-resolution simulations.

The performance of the models is summarised statistically using Taylor diagrams (a quantification of the skill score) as well as by some regional maps of the modelled SSTs and the proxy reconstructions. All three models perform extremely well between 25–50° S and 25–50° N. They are less adequate in the northern-hemisphere high latitudes and in the tropical regions. However, it is not obvious that the eddy-permitting simulation contributes significantly to the improvement of the sea-surface-state results with regard to the paleo-reconstructions. Although some differences in the structure of the "coarse-resolution" and "eddy-permitting" SSTs are noticeable in specific regions, e.g. the Agulhas and Kuroshio areas, these results may locally yield a better consistency between model and proxy data but do not contribute significantly to the global statistical score. More reconstructions are required in areas where the regional dynamics may play a key role for the surface temperature structure.

As underlined by Ballarotta et al. (2013), the simulated LGM sea-ice cover is consistent with the CCSM3 simulation undertaken by Brandefelt and Otto-Bliesner (2009), which showed an increasing trend for the sea-ice fraction (especially in the Northern Hemisphere) at the second equilibrated stage. However, the sea-ice area in the three

CPD
9, 329–350, 2013

simulations compared here is larger than those previously reported in the PMIP model analyses. The discrepancies are probably associated with the particularly large Southern Ocean sea-ice cover simulated by the CCSM model (Murakami et al., 2008) and the choice of the model equilibrium. Consequently, the seasonality of the Southern Ocean sea-ice cover is not captured by the eddy-permitting simulation and our results, as the majority of the PMIP simulation (Roche et al., 2012), are thus not fully consistent with the paleo-reconstructions.

A summary of the overall results is that this investigation indicates that a higher model resolution is not a panacea yielding the hoped-for better correspondence between simulations and proxy archives. Until more experiments, either corroborating or invalidating the results of the present study, have been undertaken, only provisional conclusions may be drawn. One of these is that as regards enhancing model performance, it may be more productive to aim at improving the parameterisations of small-scale processes rather than to focus on increasing model resolution.

Supplementary material related to this article is available online at: http://www.clim-past-discuss.net/9/329/2013/cpd-9-329-2013-supplement.zip.

Acknowledgements. This work has been financially supported by the Bert Bolin Centre for Climate Research and by the Swedish Research Council. The Swedish National Infrastructure for Computing (SNIC) is gratefully acknowledged for providing the computer time on the Vagn and Ekman facilities funded by the Knut and Alice Wallenberg foundation.

References

Ballarotta, M., Brodeau, L., Brandefelt, J., Lundberg, P., and Döös, K.: A Last Glacial Maximum world-ocean simulation at eddy-permitting resolution – Part 1: Experimental design and basic evalusation, Clim. Past Discuss., 9, 297–328, doi:10.5194/cpd-9-297-2013, 2013. 332, 336

Braconnot, P., Harrison, S. P., Kageyama, M., Bartlein, P. J., Masson-Delmotte, V., Abe-Ouchi, A., Otto-Bliesner, B., and Zhao, Y.: Evaluation of climate models using palaeoclimatic data, Nature Climate Change, 2, 417–424, doi:10.1038/NCLIMATE1456, 2012. 331

Brandefelt, J. and Otto-Bliesner, B. L.: Equilibration and variability in a Last Glacial Maximum climate simulation with CCSM3, Geophys. Res. Lett., 36, 1–5, doi:10.1029/2009GL040364, 2009. 332, 333, 336

De Vernal, A., Rosell-Mel, A., Kucera, M., Hillaire-Marcel, C., Eynaud, F., Weinelt, M., Dokken, T., and Kageyama, M.: Comparing proxies for the reconstruction of LGM sea-surface conditions in the northern North Atlantic, Quaternary Sci. Rev., 25, 2820–2834, doi:10.1016/j.quascirev.2006.06.006, 2006. 335

Gersonde, R, Crosta, X., Abelmann, A., and Armand, L.: Sea-surface temperature and sea ice distribution of the Southern Ocean at the EPILOG Last Glacial Maximum – a circum-Antarctic view based on siliceous microfossil records, Quaternary Sci. Rev., 24, 869–896, doi:10.1016/j.quascirev.2004.07.015, 2005. 335, 349, 350

Hargreaves, J. C., Paul, A., Ohgaito, R., Abe-Ouchi, A., and Annan, J. D.: Are paleoclimate model ensembles consistent with the MARGO data synthesis?, Clim. Past, 7, 917–933, doi:10.5194/cp-7-917-2011, 2011. 330, 331

Hargreaves, J. C., Annan, J. D., Ohgaito, R., Paul, A., and Abe-Ouchi, A.: Skill and reliability of climate model ensembles at the Last Glacial Maximum and mid Holocene, Clim. Past Discuss., 8, 3481–3511, doi:10.5194/cpd-8-3481-2012, 2012. 331

Kageyama, M., Laîné, A., Abe-Ouchi, A., Braconnot, P., Cortijo, E., Crucifix, A., de Vernal, A., Guiot, J., Hewitt, C., and Kitoh, A.: Last Glacial Maximum temperatures over the North Atlantic, Europe and western Siberia: a comparison between PMIP models, MARGO sea surface temperatures and pollen-based reconstructions, Quaternary Sci. Rev., 25, 2082–2102, doi:10.1016/j.quascirev.2006.02.010, 2006. 331

Madec, G.: NEMO ocean engine, France, Note du Pôle de modélisation de l'Institut Pierre-Simon Laplace No. 27 (27), 2008. 332

Murakami, S., Ohgaito, R., Abe-Ouchi, A., Crucifix, M., and Otto-Bliesner, B.: Global-scale energy and freshwater balance in glacial climate: a comparison of three PMIP2 LGM simulations, J. Climate, 21, 5008–5033, doi:10.1175/2008JCLI2104.1, 2008. 337

Nørgaard-Pedersen, N, Spielhagen, R. F., Erlenkeuser, H., Grootes, P. M., Heinemeier, J., and Knies, J.: Arctic Ocean during the Last Glacial Maximum: atlantic and polar

CPD
9, 329–350, 2013

domains of surface water mass distribution and ice cover, Paleoceanography, 18, 1–19, doi:10.1029/2002PA000781, 2003. 335

Otto-Bliesner, B., Schneider, R., Brady, E. C., Kucera, M., Abe-Ouchi, A., Bard, E., Braconnot, P. Crucifix, M., Hewitt, C. D., Kageyama, M. Marti, O., Paul, A., Rosell-Melé, A., Waelbroeck, C., Weber, S. L., Weinelt, M., and Yu, Y.: A comparison of PMIP2 model simulations and the MARGO proxy reconstruction for tropical sea surface temperatures at last glacial maximum, Clim. Dynam., 32, 799–815, doi:10.1007/s00382-008-0509-0, 2009. 331

Pflaumann, U., Sarnthein, M., Chapman, M., d'Abreu, L., Funnell, B., Huels, M., Kiefer, T. Maslin, M., Schulz, H., Swallow, J., van Kreveld, S., Vautravers, M., Vogelsang, E., and Weinelt, M.: Glacial North Atlantic: Sea-surface conditions reconstructed by GLAMAP 2000, Paleoceanography, 18, 1–21, doi:10.1029/2002PA000774, 2003. 335

Roche, D. M., Crosta, X., and H. Renssen: Evaluating Southern Ocean sea-ice for the Last Glacial Maximum and pre-industrial climates: PMIP-2 models and data evidence, Quaternary Sci. Rev., 56, 99–106, doi:10.1016/j.quascirev.2012.09.020, 2012. 337

Taylor, K. E.: Summarizing multiple aspects of model performance in a single diagram, J. Geophys. Res., 106, 7183–719, doi:10.1029/2000JD900719, 2001. 332, 333, 341

Waelbroeck, C., Paul, A., Kucera, M., Rosell-Melé, A., Weinelt, M., Schneider, R., Mix, A. C., Abelmann, A., Armand, L., Bard, E., Barker, S., Barrows, T. T., Benway, H., Cacho, I., Chen, M.-T., Cortijo, E., Crosta, X., de Vernal, A., Dokken, T., Duprat, J., Elderfield, H., Eynaud, F., Gersonde, R., Hayes, A., Henry, M., Hillaire-Marcel, C., Huang, C.-C., Jansen, E., Juggins, S., Kallel, N., Kiefer, T., Kienast, M., Labeyrie, L., Leclaire, H., Londeix, L., Mangin, S., Matthiessen, J., Marret, F., Meland, M., Morey, A. E., Mulitza, S., Pflaumann, U., Pisias, N. G., Radi, T., Rochon, A., Rohling, E. J., Sbaffi, L., Schäfer-Neth, C., Solignac, S., Spero, H., Tachikawa, K., and Turon, J.-L.: Constraints on the magnitude and patterns of ocean cooling at the Last Glacial Maximum, Nat. Geosci., 2, 127–132, doi:10.1038/NGEO411, 2009. 331, 332, 333

CPD
9, 329–350, 2013

Table 1. Comparison of the LGM designed configurations, model version, atmospheric forcing variables and their frequency (d days, h hours and m months), bottom and surface conditions.

Model	NEMO-ORCA025	NEMO-ORCA1	CCSM3
Horizontal resolution	$\approx 0.25^\circ \times 0.25^\circ$	$\approx 1^\circ \times 1^\circ$	$\approx 1^\circ \times 1^\circ$
Vertical resolution	46 depth levels	64 depth levels	40 depth levels
Atmospheric forcing	GFS1.0	GFS1.0	COUPLED
frequency u_{10}	6 h	6 h	
frequency v_{10}	6 h	6 h	
frequency rad_{sw}	1 d	1 d	
frequency rad_{lw}	1 d	1 d	
frequency t_2	6 h	6 h	
frequency q_2	6 h	6 h	
frequency precip	1 d	1 d	
frequency snow	1 d	1 d	
frequency runoff	1 d	1 d	
Bathymetry	ICE-5G	ICE-5G	ICE-5G
Coupling ocean/sea-ice	every 2 h	every 2 h	once a day

CPD
9, 329–350, 2013

Table 2. Skill scores as defined by Taylor (2001) for the NEMO-ORCA025, NEMO-ORCA1 and CCSM3 experiments.

	NEMO-ORCA025			NEMO-ORCA1			CCSM3		
	Annual	Winter (JFM)	Summer (JAS)	Annual	Winter (JFM)	Summer (JAS)	Annual	Winter (JFM)	Summer (JAS)
50° N–90° N	0.01	0.01	0.04	0.02	0.03	0.04	0.05	0.04	0.16
25° N–50° N	0.83	0.92	0.90	0.87	0.95	0.92	0.86	0.94	0.88
25° S–25° N	0.55	0.63	0.62	0.56	0.66	0.63	0.56	0.66	0.63
25° S–50° S	0.97	0.98	0.97	0.97	0.98	0.97	0.97	0.98	0.97

CPD
9, 329–350, 2013

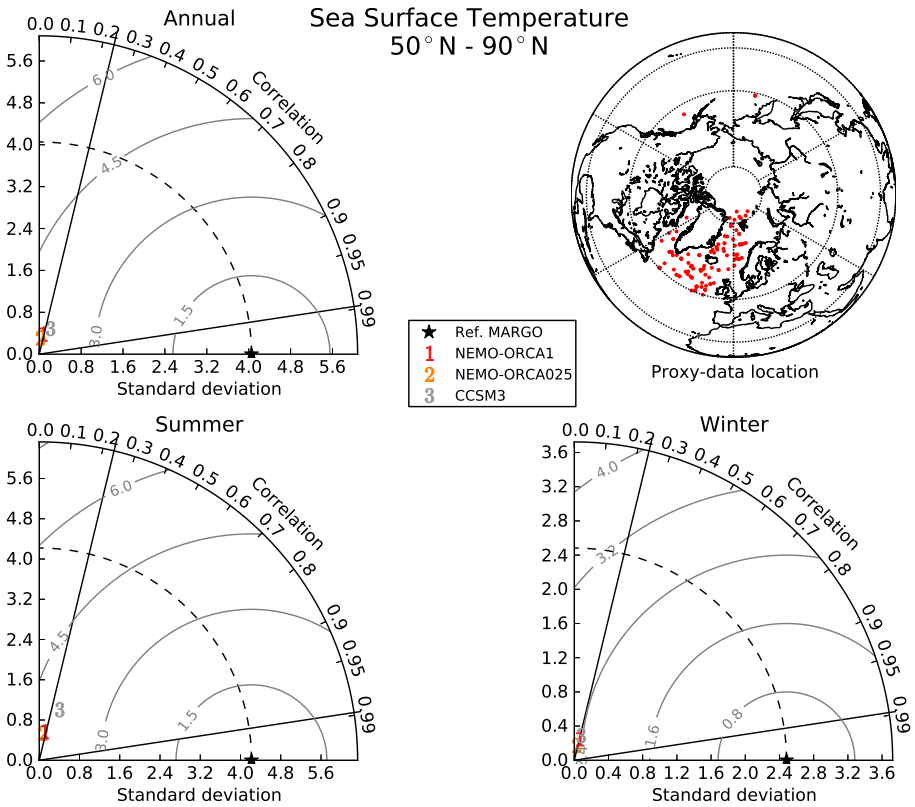

Fig. 1. Taylor diagrams for the annual, boreal winter (JFM) and boreal summer (JAS) LGM sea surface temperature between 50 and 90° N. The proxy-data locations are shown in the upper right-hand diagram.

CPD
9, 329–350, 2013

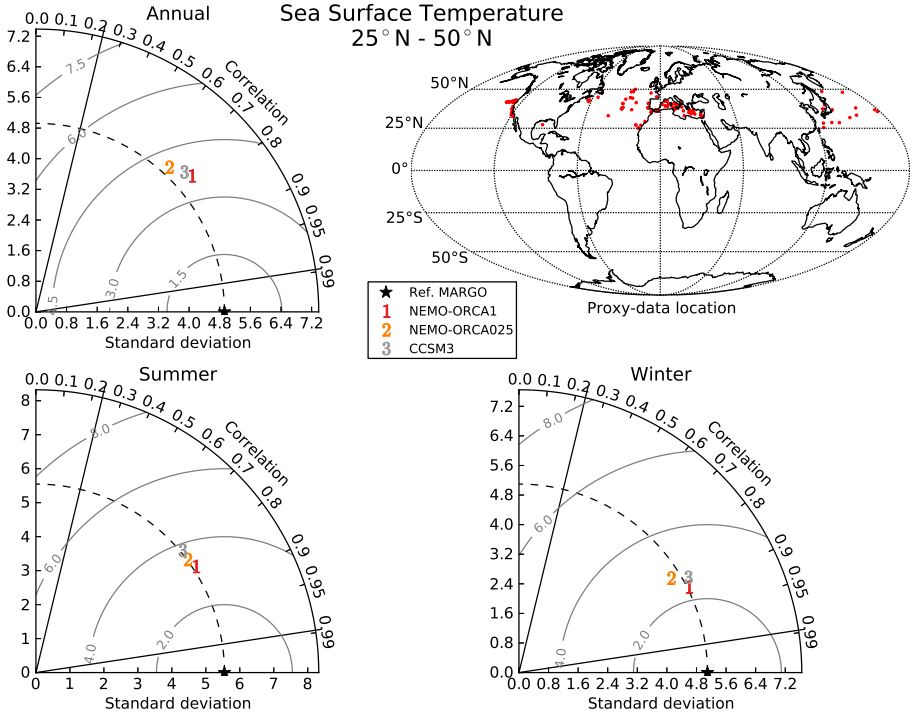

Fig. 2. Taylor diagrams for the annual, boreal winter (JFM) and boreal summer (JAS) LGM sea surface temperature between 25 and 50° N. The proxy-data locations are shown in the upper right-hand diagram.

CPD
9, 329–350, 2013

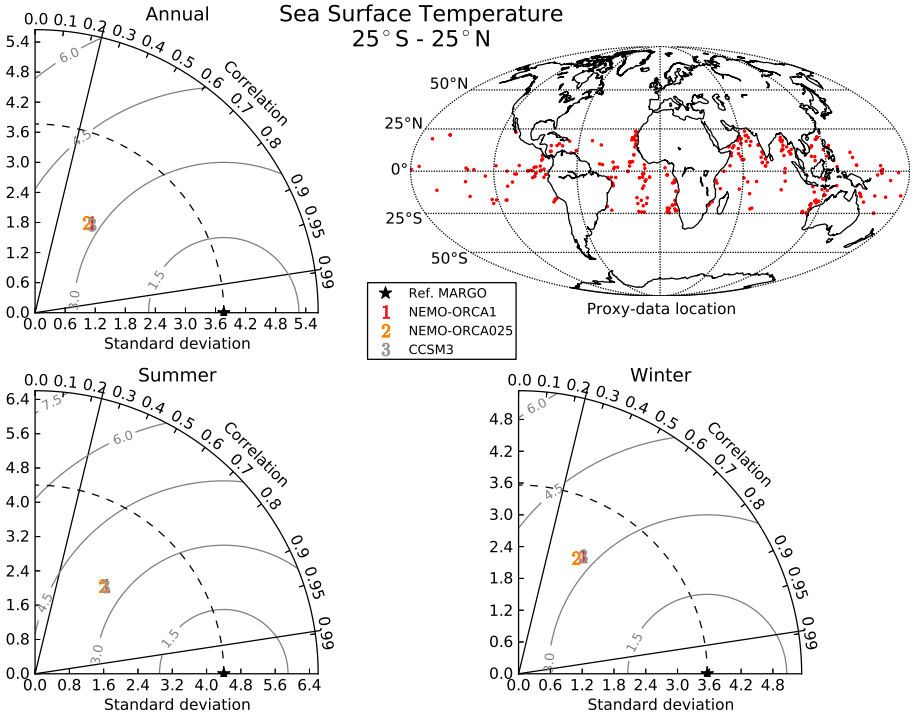

Fig. 3. Taylor diagrams for the annual, boreal winter (JFM) and boreal summer (JAS) LGM sea surface temperature between 25° S and 25° N. The proxy-data locations are shown in the upper right-hand diagram.

CPD
9, 329–350, 2013

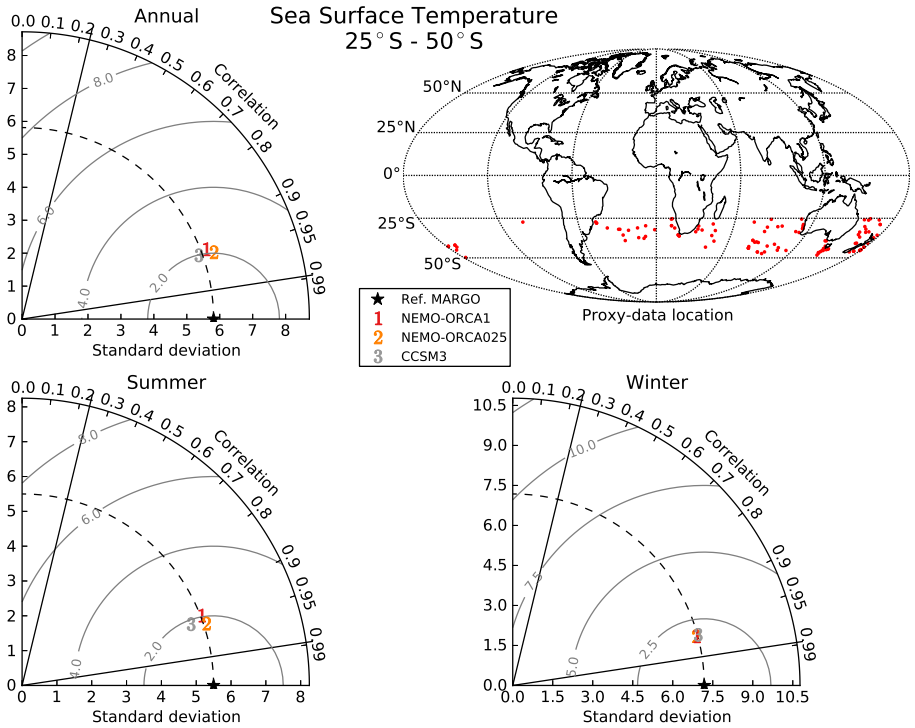

Fig. 4. Taylor diagrams for the annual, boreal winter (JFM) and boreal summer (JAS) LGM sea surface temperature between 25 and 50° S. The proxy-data locations are shown in the upper right-hand diagram.

CPD
9, 329–350, 2013

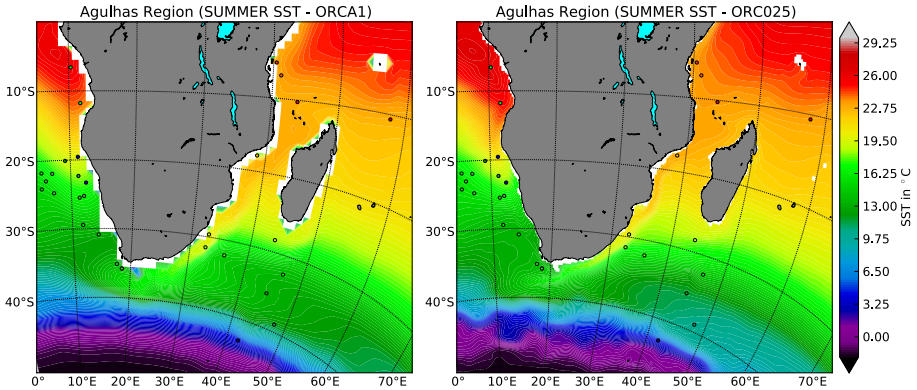

Fig. 5. NEMO-ORCA1 and NEMO-ORCA025 sea surface temperature (SST) maps in the Agulhas region superimposed on the proxy-data locations in the MARGO reconstruction.

CPD
9, 329–350, 2013

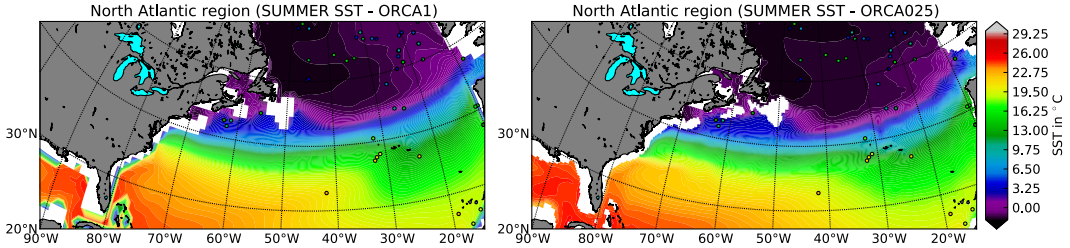

Fig. 6. NEMO-ORCA1 and NEMO-ORCA025 sea surface temperature (SST) maps in the North Atlantic region superimposed on the proxy-data locations in the MARGO reconstruction.

CPD
9, 329–350, 2013

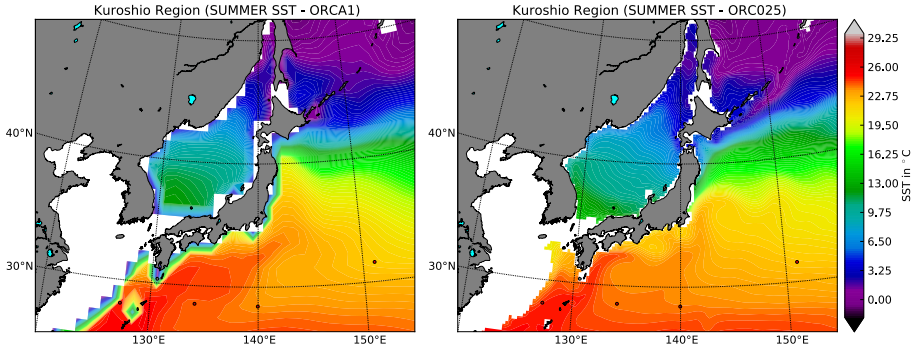

Fig. 7. NEMO-ORCA1 and NEMO-ORCA025 sea surface temperature (SST) maps in the Kuroshio region superimposed on the proxy-data locations in the MARGO reconstruction.

CPD
9, 329–350, 2013

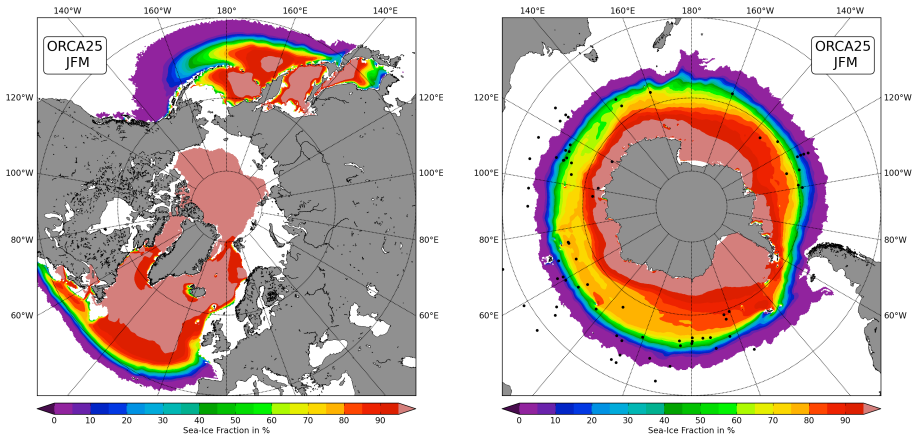

Fig. 8. Polar stereographic maps of the sea-ice fraction in % as simulated by the NEMO-ORCA025 LGM experiment for the boreal winter months. The locations of the Southern Ocean paleo-reconstructions from Gersonde et al. (2005) are superimposed.

CPD
9, 329–350, 2013

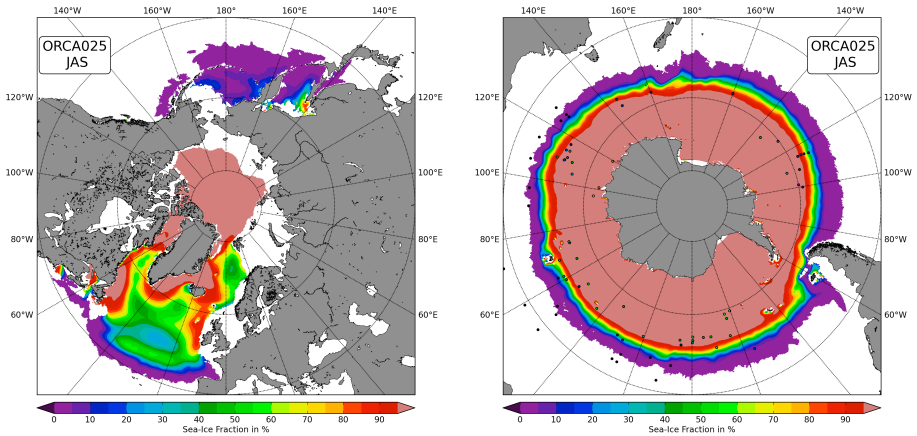

Fig. 9. Polar stereographic maps of the sea-ice fraction in % as simulated by the NEMO-ORCA025 LGM experiment for the boreal summer months. The locations of the Southern Ocean paleo-reconstructions from Gersonde et al. (2005) are superimposed.

CPD
9, 329–350, 2013